SUPPLEMENTARY INFORMATION

Low-Surface-Energy Nanofillers for Fast and Selective Li^+ Transport toward Stable Solid-State Lithium Metal Batteries

Jie Yang,[#a] Wenqiang Han,[#a] Yanfei Yang,*[a,b] La Zhuo[a] and Junping Zhang*[a,b]

[a] Research Center of Resource Chemistry and Energy Materials, Lanzhou Institute of Chemical Physics, Chinese Academy of Sciences, 730000 Lanzhou, P. R. China

[b] Center of Materials Science and Optoelectronics Engineering, University of Chinese Academy of Sciences, 100049 Beijing, P. R. China

[#] This author has contributed equally to this work

*E-mail: yangyf@licp.cas.cn, jpzhang@licp.cas.cn

EXPERIMENTAL SECTION

1.1 Materials

SiO_2 nanoparticles were obtained from Hubei Huifu Nanomaterial Co., Ltd. and dried under vacuum at 105 °C overnight before use. Vinyltrichlorosilane (98%) was purchased from Gelest. Poly(ethylene oxide) (PEO, M_n = 600 000 g mol^{-1}), succinonitrile (SN), and acetonitrile were purchased from Sigma-Aldrich. Lithium bis(trifluoromethanesulfonyl) imide (LiTFSI, 99.8%) was supplied by Dodo Chem (China). $LiFePO_4$ (LFP), Super P carbon, polyvinylidene difluoride (PVDF), N-methyl-2-pyrrolidone, carbon-coated aluminum foil, lithium metal (400 μm), and ultrathin Li foils (50 μm) were obtained from Guangdong Canrd Technology Co., Ltd. (China). All other reagents of analytical grade were provided by China National Medicines Co., Ltd.

1.2 Preparation of SE@$SiO_{2(x)}$ Nanofillers

0.1 g of SiO_2 nanoparticles (~7 nm in diameter, specific surface area 300 m^2 g^{-1}) were dispersed in 80 mL of toluene under vigorous stirring. The water content of the suspension was adjusted to 120, 160, 200, 240, or 280 ppm by flowing dry or humid N_2 to control the hydrolytic condensation environment of VTCS. Then, 200 μL of VTCS was added, and the mixture was stirred at room temperature for 24 h. The resulting precipitate was collected by centrifugation, washed repeatedly with toluene (20 mL) and ethanol (20 mL), and dried at 105 °C. The products were denoted as SE@$SiO_{2(x)}$, where x represents the water concentration in toluene.

1.3 Preparation of PEO/SE@$SiO_{2(x)}$ CSEs

The PEO/SE@$SiO_{2(x)}$ CSEs were fabricated by solution casting and solvent evaporation. A prescribed amount of the SE@$SiO_{2(x)}$ nanofiller was dispersed in 7.0 mL of acetonitrile by ultrasonication (650 W, 20 min), followed by stirring (4 h) to obtain a homogeneous

suspension. To this, 0.433 g of PEO, 0.250 g of succinonitrile, and 0.110 g of LiTFSI were added and stirred at room temperature for 24 h. The resulting slurry was cast onto a polytetrafluoroethylene substrate and dried under vacuum at 30 °C for 12 h to form the flexible CSEs. The filler loading ranged from 15 to 17 wt% relative to the total mass of PEO and SE@$SiO_{2(x)}$. For comparison, the PEO/SiO_2 CSE was also prepared under identical conditions.

1.4 Preparation of the Cathode

The LFP cathode slurry was prepared by mixing 1.20 g of LFP, 0.30 g of Super P, 0.30 g of PVDF, 0.12 g of PEO, 0.10 g of SN, and 0.10 g of LiTFSI in N-methyl-2-pyrrolidone, followed by grinding in an agate mortar for 120 min. The homogeneous slurry was uniformly coated onto carbon-coated Al foil and vacuum-dried at 80 °C for 24 h to ensure complete solvent removal. The areal loading of active materials was 1.0 mg cm^{-2}.

1.5 Assembly of the Pouch Cell

The composite cathode was fabricated by casting the PEO/SE@$SiO_{2(200)}$ slurry onto the pre-formed LFP cathode (LFP loading: 1.0 mg cm^{-2}). A high-purity Li foil (50 µm) served as the anode. The pouch cell was assembled by stacking the Li anode and the LFP@PEO/SE@$SiO_{2(200)}$ composite cathode under a dry argon atmosphere.

1.6 Electrochemical Measurements

Electrochemical impedance spectroscopy of Li/stainless steel cells was performed on a CHI660E workstation with an amplitude of 10 mV in the frequency range of 10^6–0.1 Hz. The total ionic conductivity was calculated using equation (1):

$$\sigma = d/(A * R_{bulk}) \quad (1)$$

where d is electrolyte thickness (cm), A is electrode area (1.77 cm^2), and R_{bulk} is bulk resistance (Ω).

The activation energy (E_a) was determined from the Arrhenius relationship:

$$\sigma = A \exp(-E_a/RT) \quad (2)$$

where R is the gas constant (8.314 J mol^{-1} K^{-1}) and T is temperature (K).

The Li^+ transference number (t_{Li^+}) was determined in Li/electrolyte/Li symmetric cells under a 10 mV DC bias, using equation (3):

$$t_{Li^+} = (I_S*(\Delta V - I_0*R_0))/(I_0*(\Delta V - I_S*R_S)) \quad (3)$$

where I_o and I_s denote the initial and steady-state currents, and R_o and R_s represent the corresponding interfacial resistances.

The electrochemical stability windows were determined by linear sweep voltammetry on Li/stainless steel cells in the range of 2.0~6.0 V at a scan rate of 5 mV s^{-1}.

1.7 Characterization

The morphologies of samples were examined using TEM (TECNAI-G2-F30, FEI) and SEM (JSM-6701F, JEOL). XRD patterns were collected using a PANalytical X'pert PRO diffractometer (Cu Kα, 40 kV, 30 mA, scan range 5–35°, 2θ, 2° min^{-1}). FTIR spectra were recorded on a Nicolet NEXUS spectrometer with KBr pellets after vacuum-drying the samples at 105 °C for 12 h. Raman spectra were acquired using a LabRAM HR Evolution spectrometer (HORIBA Jobin Yvon, 532 nm laser). DSC analysis was performed on a TA Q1000 under Ar from –65 to 65 °C at a heating rate of 10 °C min^{-1}. Zeta potentials of samples in acetonitrile were measured using a Malvern ZEN3600 analyzer. Water contact angles (10 μL) were measured at 25 °C with an OCA 20 goniometer (Dataphysics). Unless otherwise stated, all measurements were performed at ambient temperature.

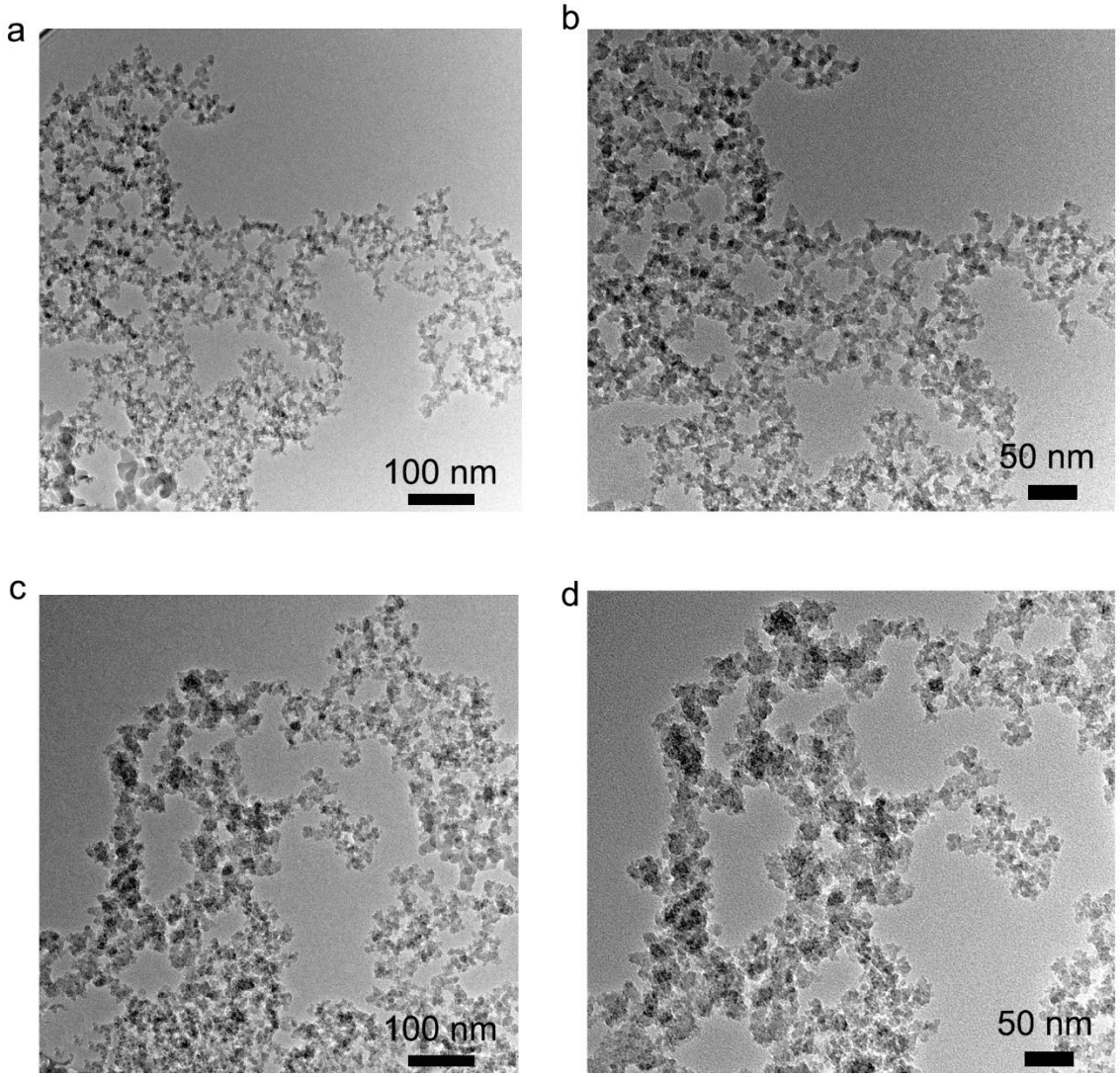

Figure S1. TEM images of (a, b) SiO_2 and (c, d) $SE@SiO_{2(200)}$.

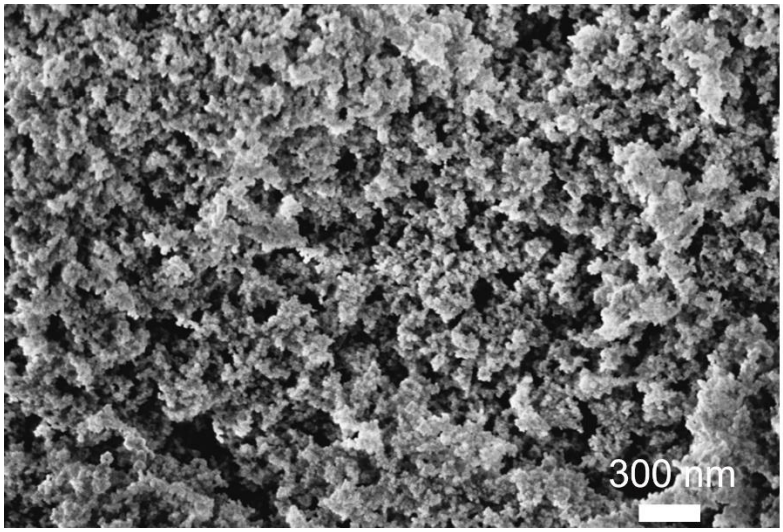

Figure S2. SEM image of $SE@SiO_{2(200)}$.

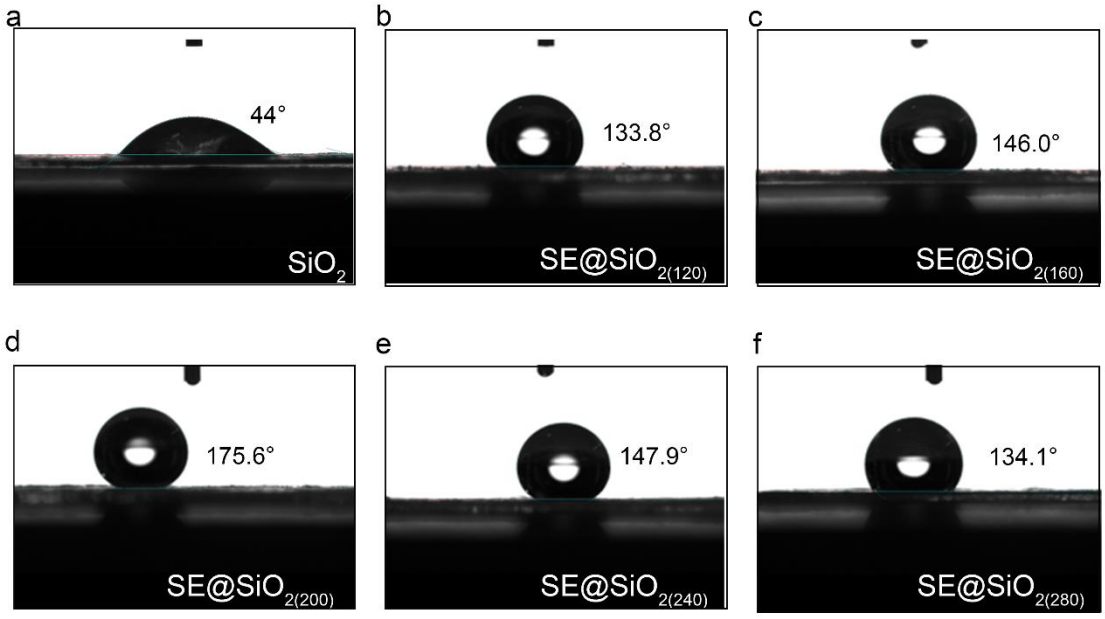

Figure S3. Contact angle of water droplets (10 µL) on the surface of (a) SiO_2, (b) $SE@SiO_{2(120)}$, (c) $SE@SiO_{2(160)}$, (d) $SE@SiO_{2(200)}$, (e) $SE@SiO_{2(240)}$, and (f) $SE@SiO_{2(280)}$.

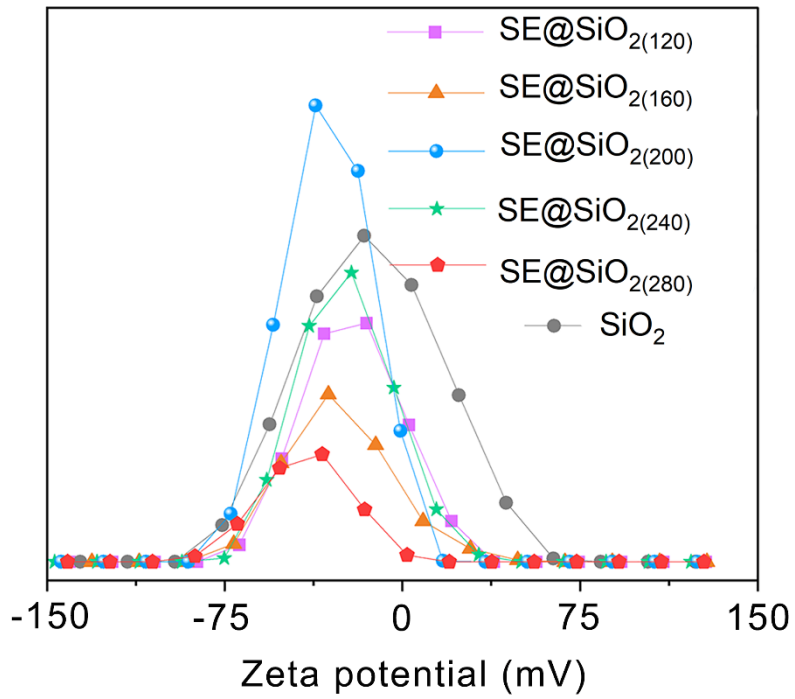

Figure S4. Zeta potential of SE@$SiO_{2(x)}$ and SiO_2 in acetonitrile.

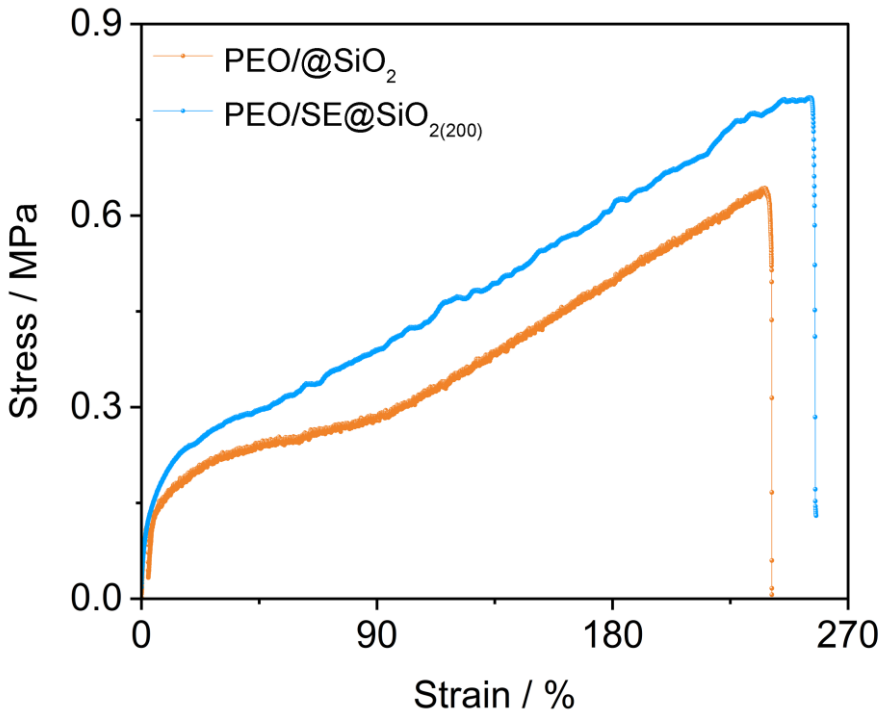

Figure S5. Stress-strain curve of different CSEs.

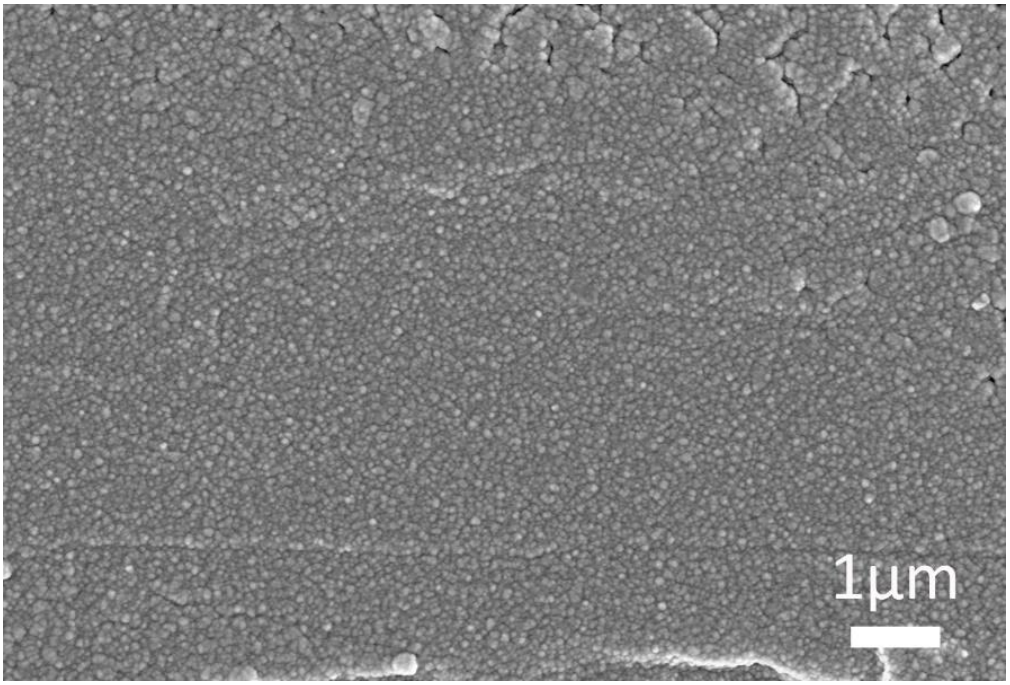

Figure S6. Cross-sectional SEM image of the PEO/SE@$SiO_{2(200)}$ CSE.

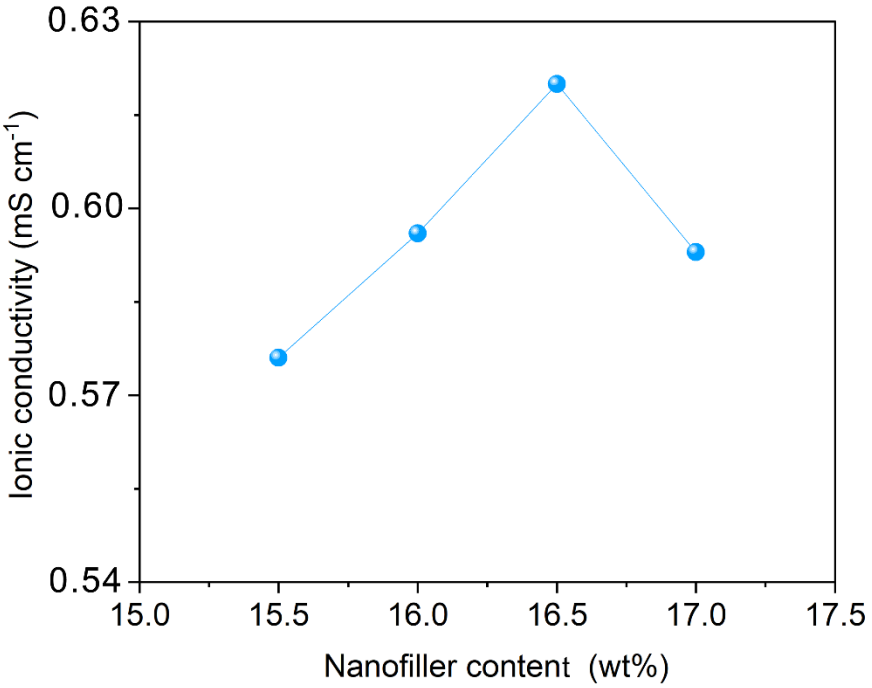

Figure S7. Ionic conductivity of PEO/SE@$SiO_{2(200)}$ CSEs as a function of the SE@$SiO_{2(200)}$ nanofiller content.

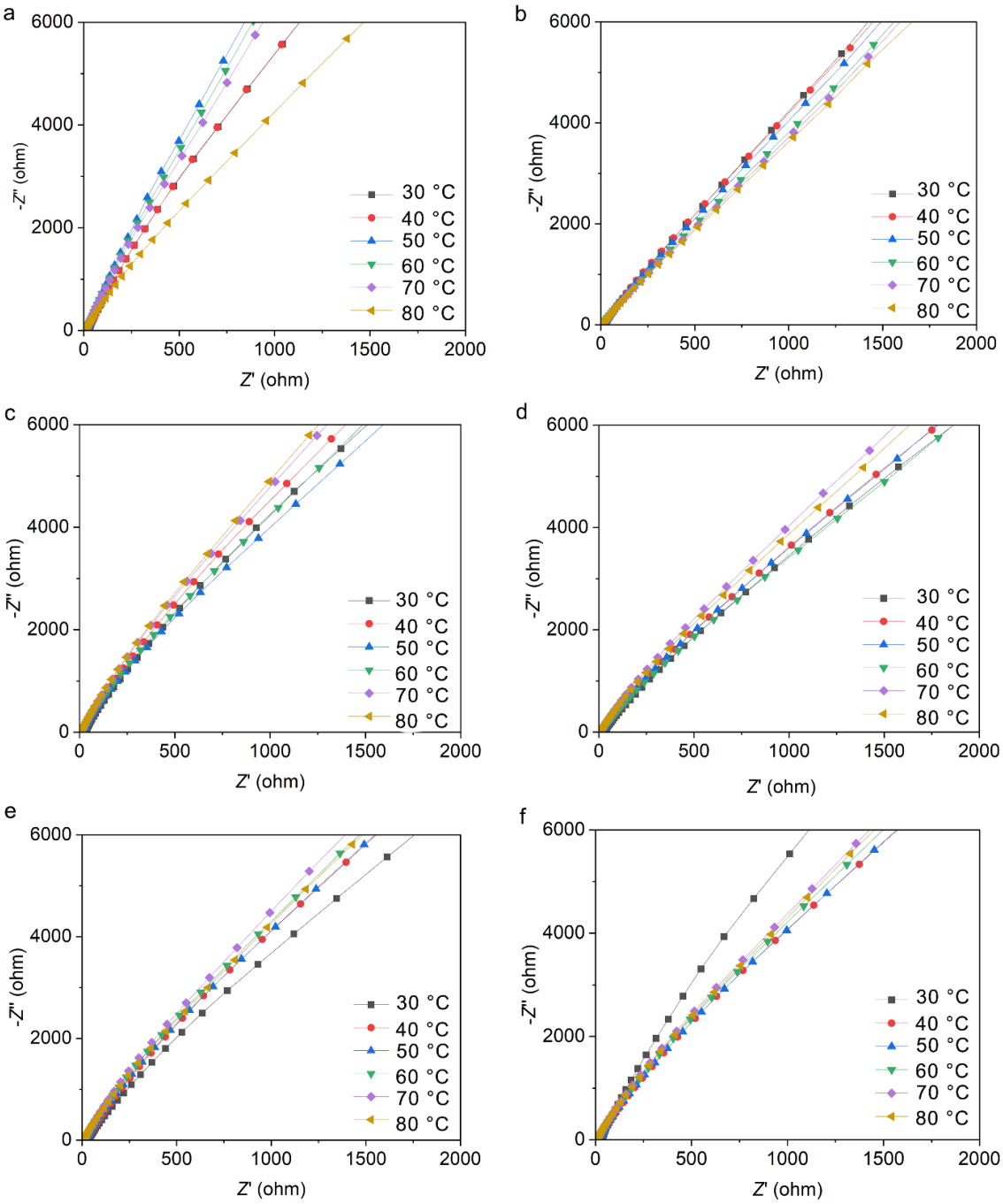

Figure S8. Calculation of the ionic conductivity and E_a. Nyquist spectra of various CSEs: (a) PEO/SiO_2, (b) PEO/SE@$SiO_{2(120)}$, (c) PEO/SE@$SiO_{2(160)}$, (d) PEO/SE@$SiO_{2(200)}$, (e) PEO/SE@$SiO_{2(240)}$, and (f) PEO/SE@$SiO_{2(280)}$.

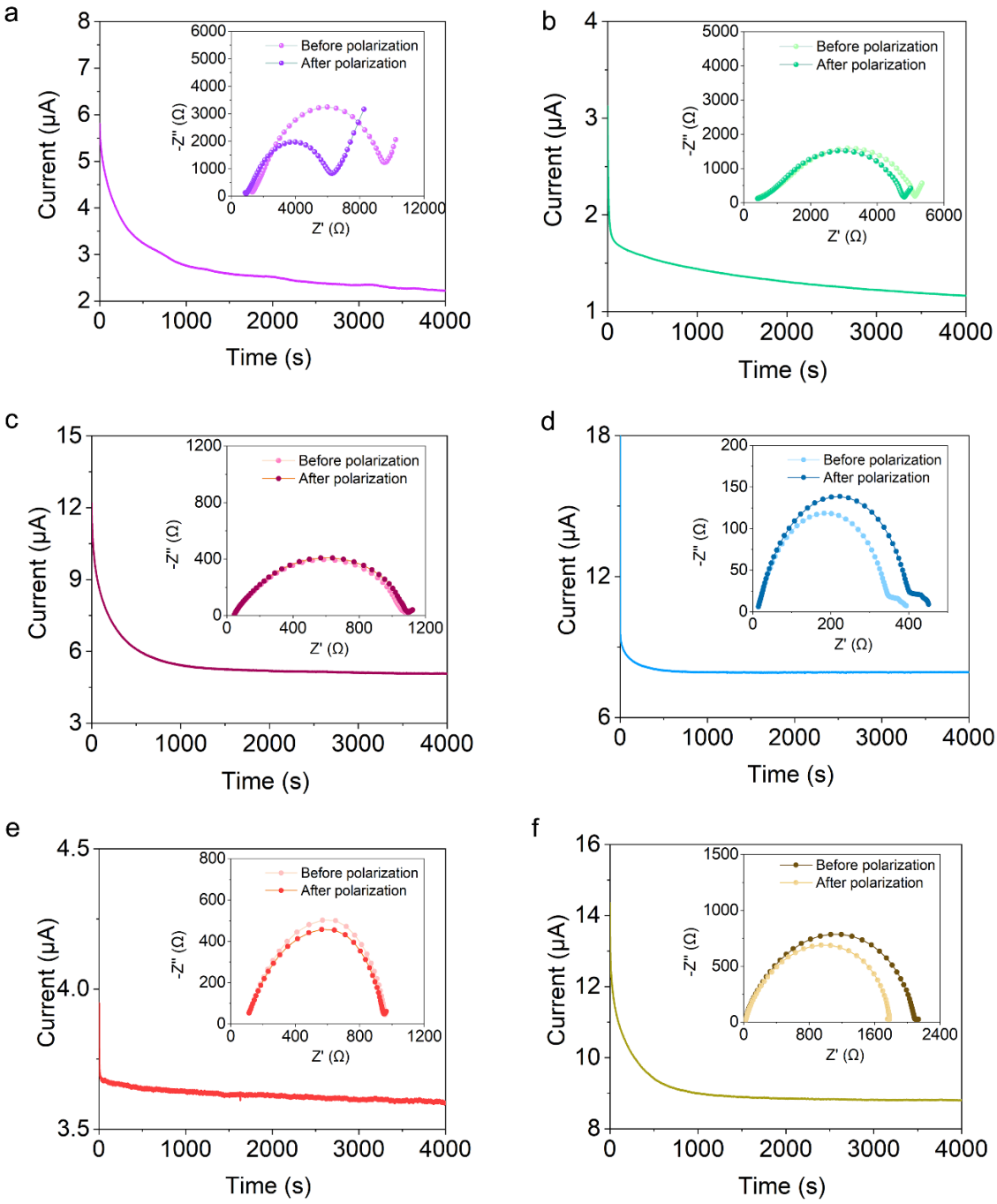

Figure S9. Calculation of the t_{Li+}. Current variations with time during polarization and the corresponding Nyquist plots of the cells assembled with the (a) PEO/SiO_2, (b) PEO/SE@$SiO_{2(120)}$, (c) PEO/SE@$SiO_{2(160)}$, (d) PEO/SE@$SiO_{2(200)}$, (e) PEO/SE@$SiO_{2(240)}$, and (f) PEO/SE@$SiO_{2(280)}$ CSEs.

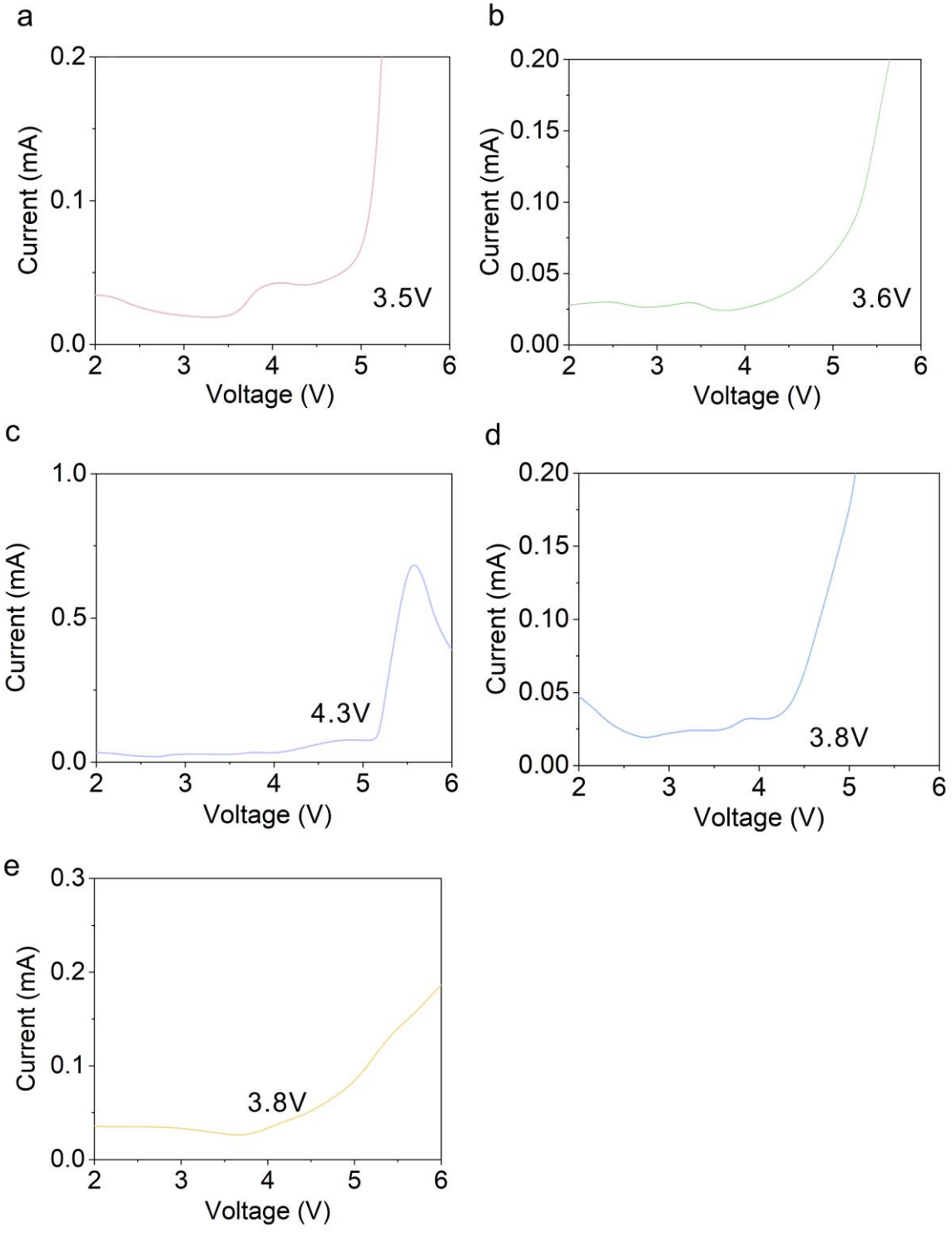

Figure S10. Linear sweep voltammetry profiles of the Li/stainless steel cells with the (a) PEO/SE@$SiO_{2(120)}$, (b) PEO/SE@$SiO_{2(160)}$, (c) PEO/SE@$SiO_{2(200)}$, (d) PEO/SE@$SiO_{2(240)}$, and (e) PEO/SE@$SiO_{2(280)}$ CSEs.

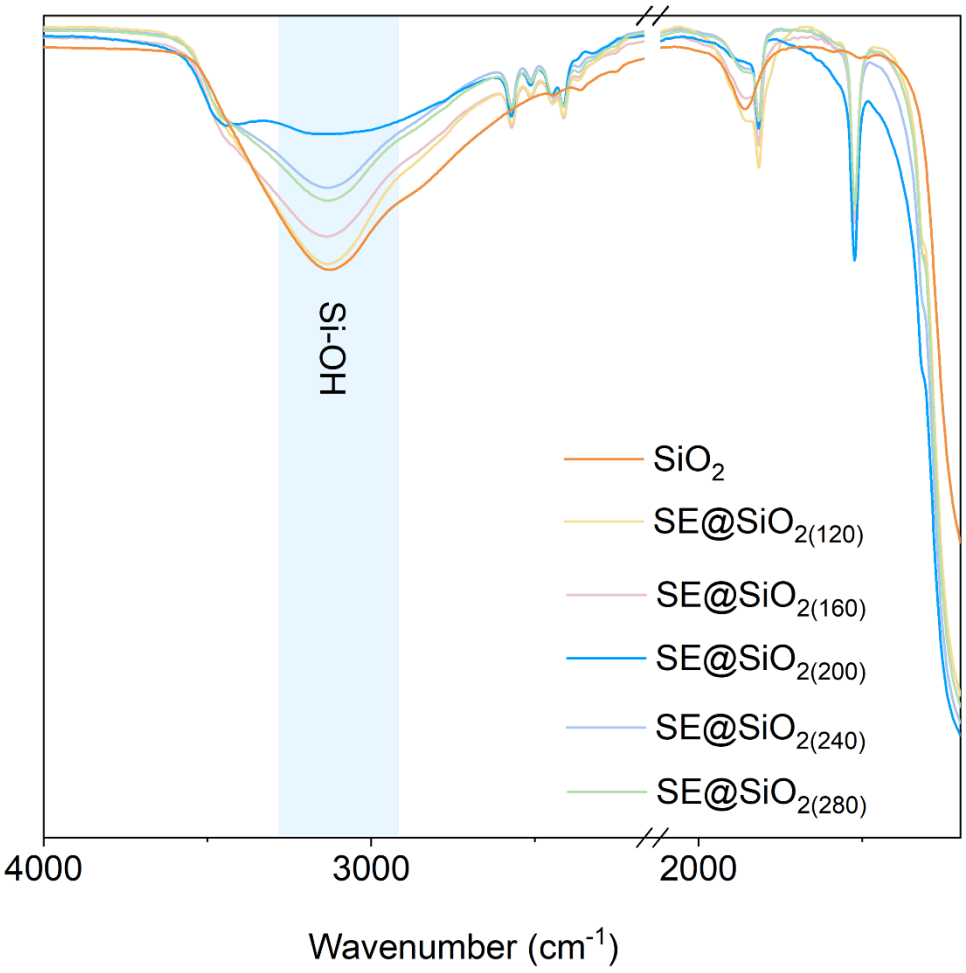

Figure S11. FTIR spectra of SiO_2 and $SE@SiO_{2(x)}$.

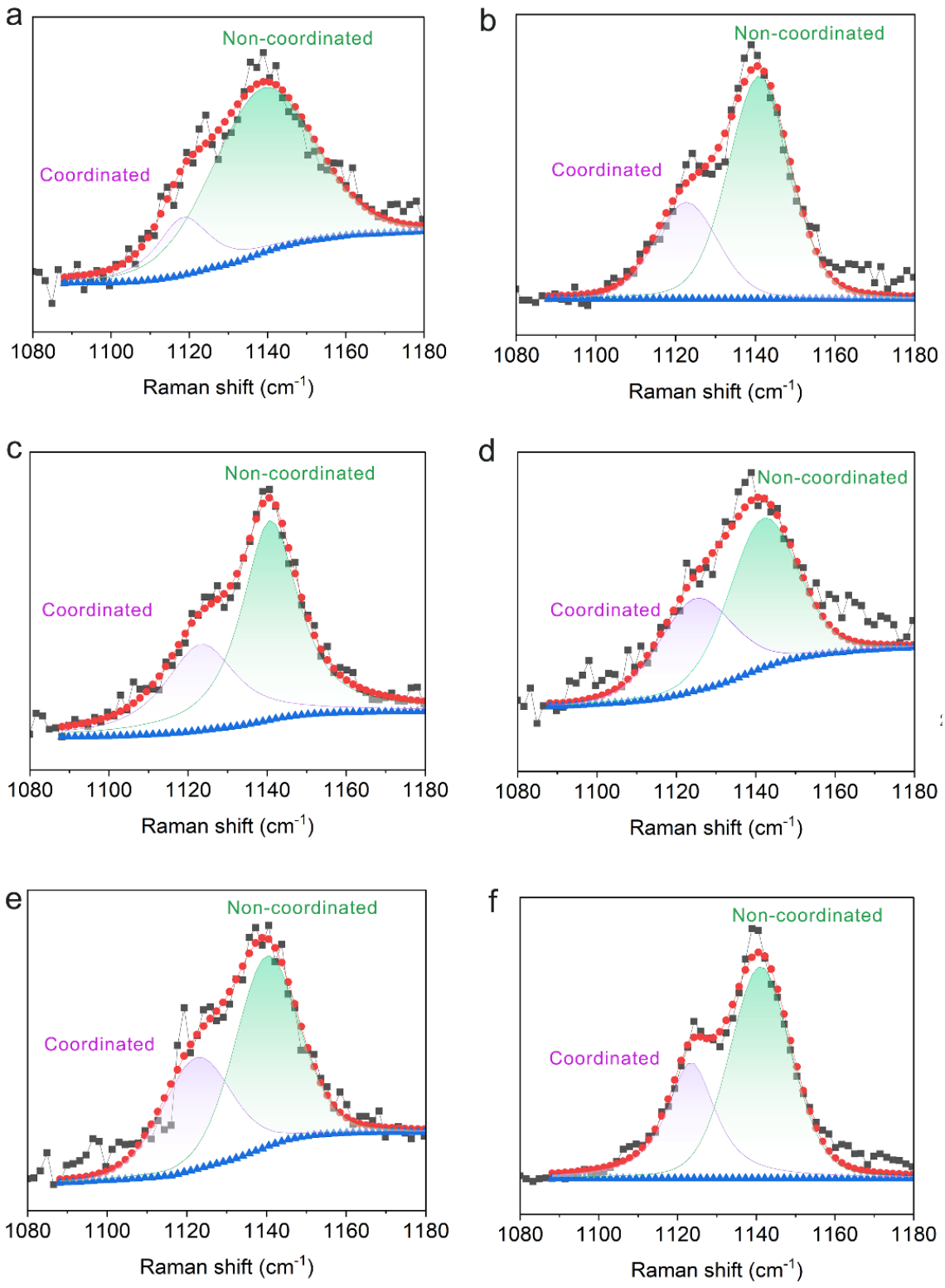

Figure S12. Raman spectra of the (a) PEO/SiO_2, (b) PEO/SE@$SiO_{2(120)}$, (c) PEO/SE@$SiO_{2(160)}$, (d) PEO/SE@$SiO_{2(200)}$, (e) PEO/SE@$SiO_{2(240)}$, and (f) PEO/SE@$SiO_{2(280)}$ CSEs.

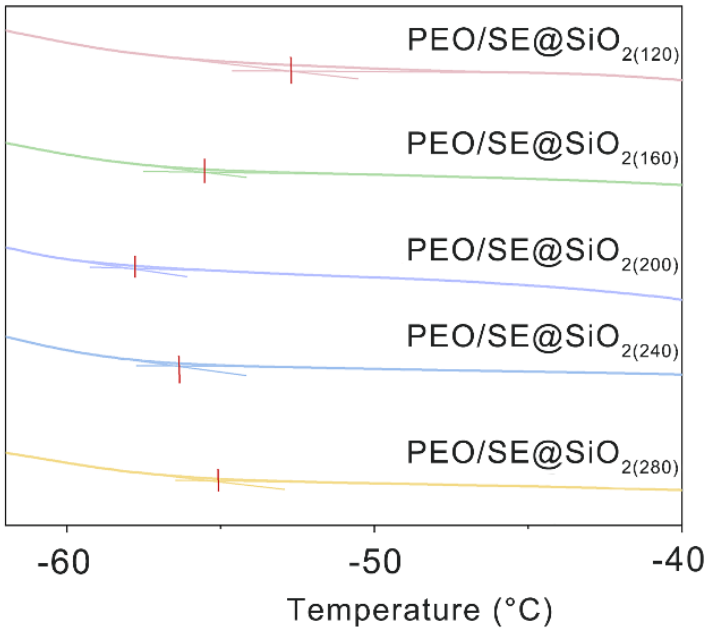

Figure S13. DSC curves of the PEO/SE@$SiO_{2(x)}$ CSEs.

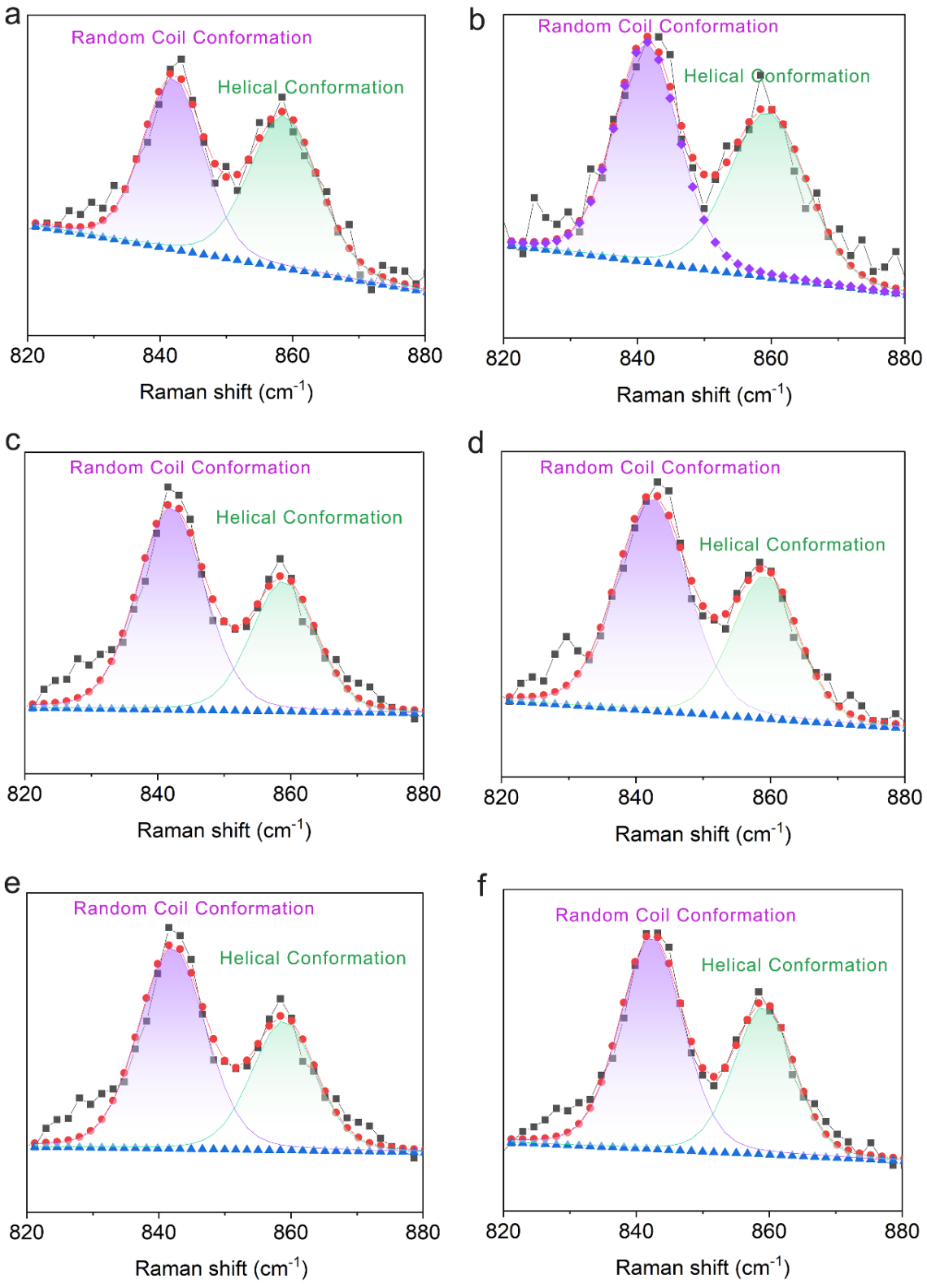

Figure S14. Raman spectra of the (a) PEO/SiO_2, (b) PEO/SE@$SiO_{2(120)}$, (c) PEO/SE@$SiO_{2(160)}$, (d) PEO/SE@$SiO_{2(200)}$, (e) PEO/SE@$SiO_{2(240)}$, and (f) PEO/SE@$SiO_{2(280)}$ CSEs.

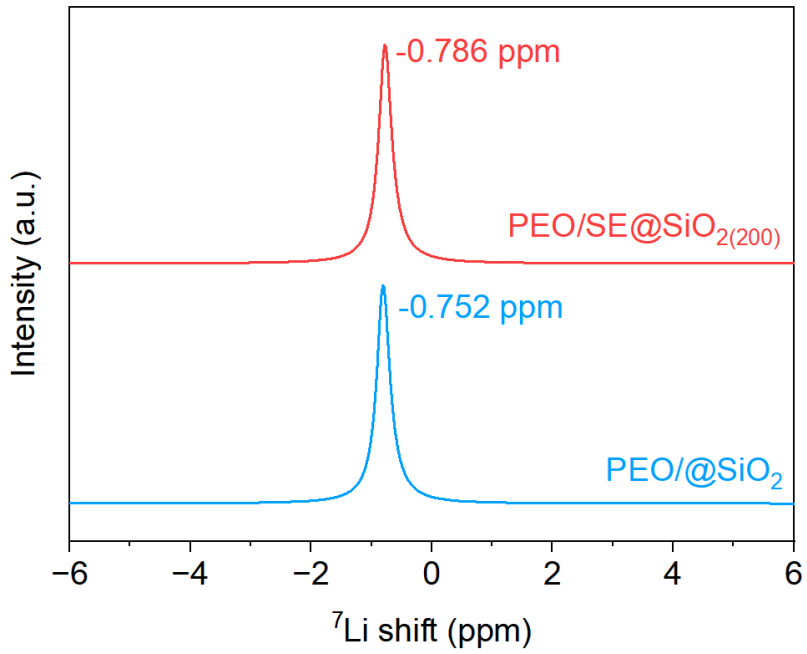

Figure S15. Solid-state ^{7}Li NMR spectra of the PEO/SiO_2 and PEO/SE@$SiO_{2(200)}$ CSEs.

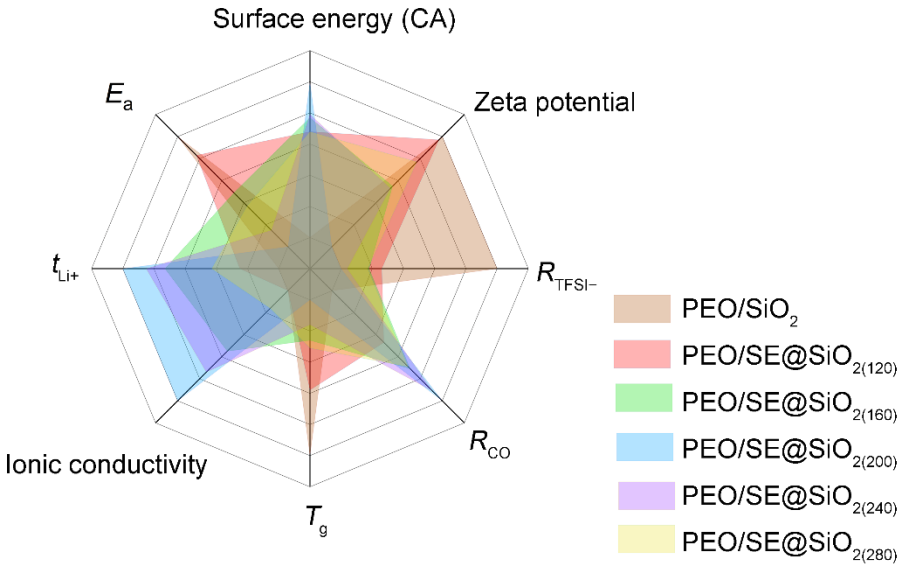

Figure S16. Summary plot correlating the apparent surface-energy descriptor, zeta potential, $TFSI^-$ coordination ratio (R_{TFSI-}), Li^+-EO coordination ratio (R_{CO}), glass-transition temperature (T_g), total ionic conductivity, and Li^+ transference number (t_{Li+}) of the PEO/SiO_2 and PEO/SE@$SiO_{2(x)}$ CSEs.

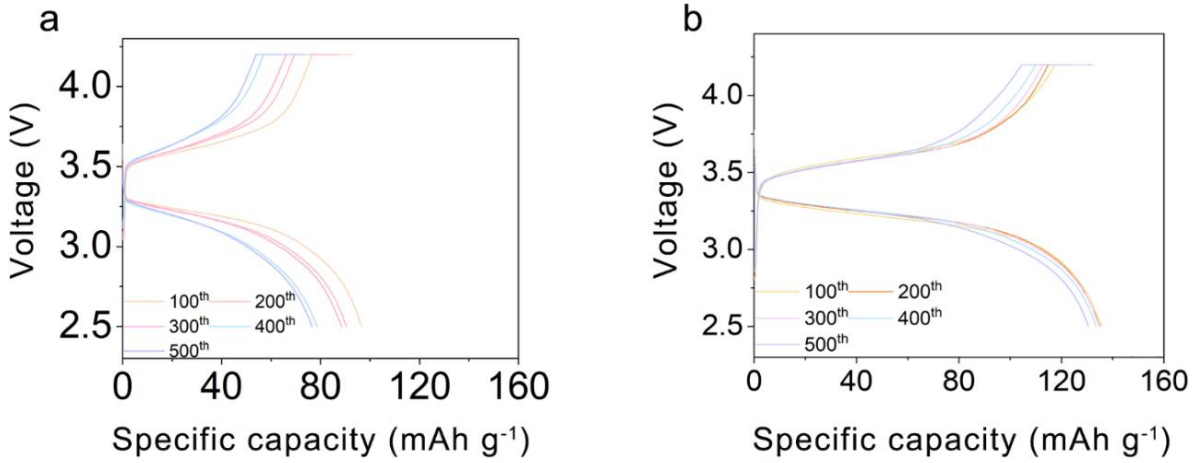

Figure S17. Discharge-charge curves of the Li/LFP cells with the (a) PEO/SiO_2 CSE and (b) PEO/SE@$SiO_{2(200)}$ CSE.

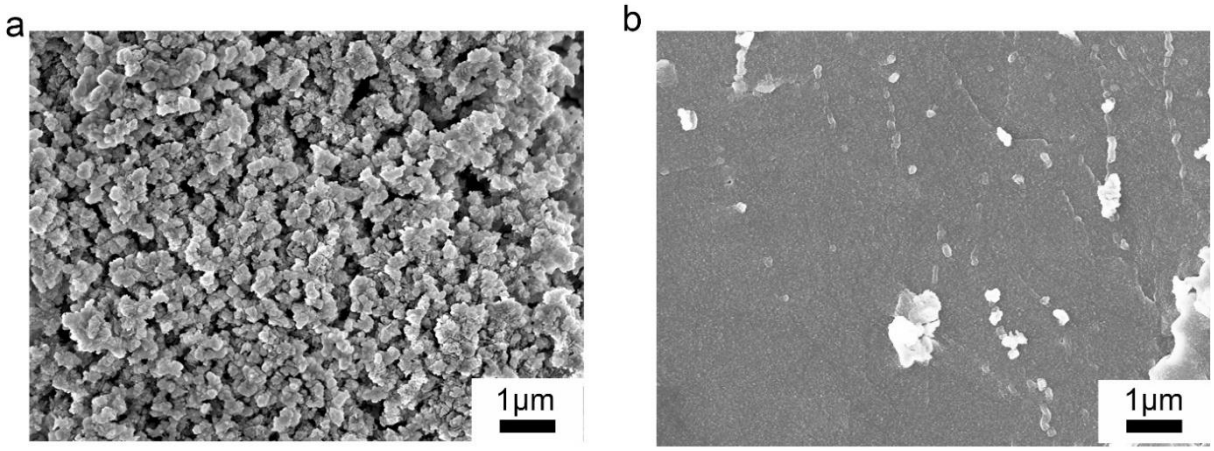

Figure S18. SEM images of the cycled Li metal anode in Li/LFP cells with the (a) PEO/SiO_2 CSE and (b) PEO/SE@$SiO_{2(200)}$ CSE.

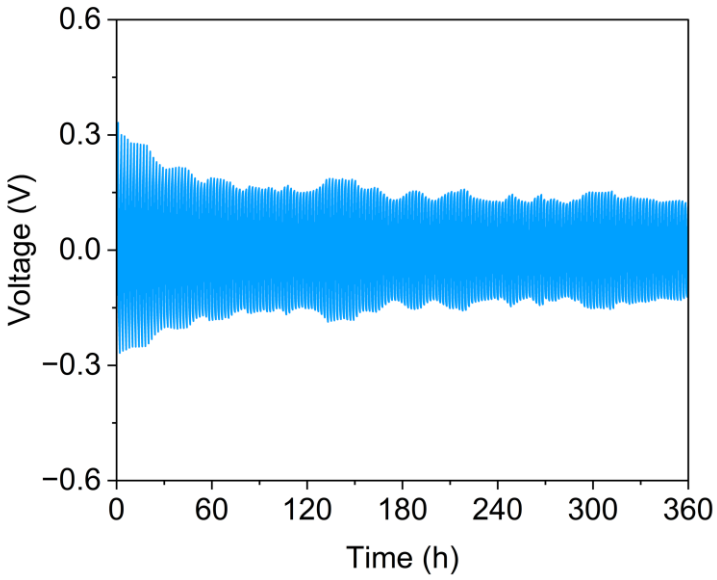

Figure S19. Cycling stability of Li symmetric cell using the PEO/SE@$SiO_{2(200)}$ CSE at 0.5 mA cm^{-2} and 0.5 mAh cm^{-2}.

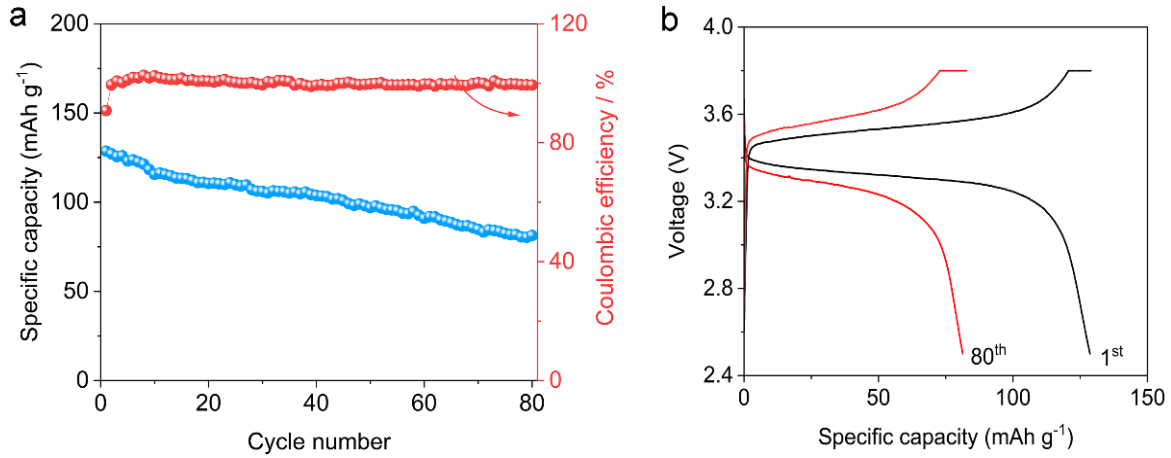

Figure S20. (a) Cycling stability and (b) discharge-charge profiles of high-loading Li||LFP cells (5.1 mg cm^{-2}) with the PEO/SE@$SiO_{2(200)}$ CSE at 0.1 C and 30 °C.

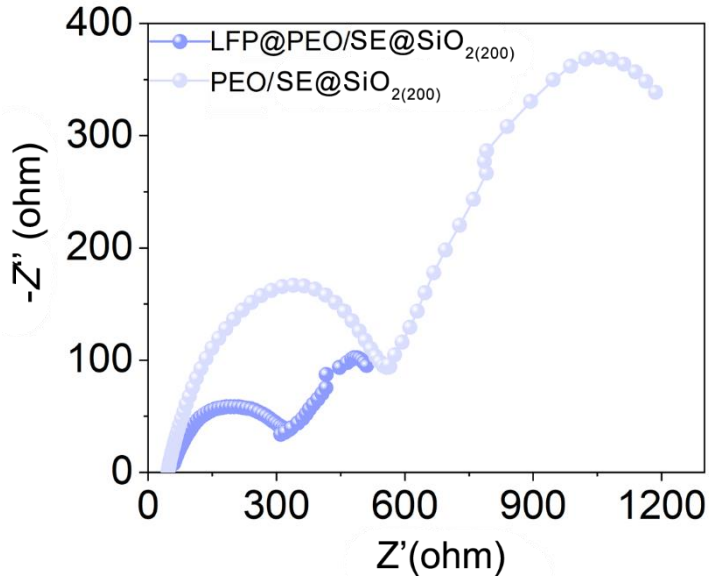

Figure S21. Nyquist spectra of the coin cells with the integrated Li/LFP@PEO/SE@$SiO_{2(200)}$ cell and conventional Li/LFP cell with PEO/SE@$SiO_{2(200)}$ CSE.

Table S1. Performances comparison of the CSEs in this work and recent studies.

CSEs	Ionic conductivity (mS cm^{-1})	t_{Li+}	Temperature (°C)	Electrochemical stability window (V)	Refs.
PEO/SE@$SiO_{2(200)}$	0.62	0.81	30	4.3	This Work
PEO/L-Li[a]	0.13	0.42	25	4.7	[1]
PEO/CuF_2	0.42	0.2	30	4.6	[2]
PEO/Mg-Al[b]	0.67	0.23	30	4.8	[3]
PEO/ZCNF[c]	0.62	0.49	60	4.51	[4]
PEO/SNFs@MMT[d]	0.49	0.62	30	5.3	[5]
GPE[e]	0.48	0.22	30	4.24	[6]
PVDF/ HTIT-37[f]	0.43	0.86	25	5.2	[7]
PEO/LSM[g]	0.252	0.75	30	5.2	[8]
PVDF/LiFSI/zeolite	0.45	0.47	25	-	[9]

[a] Single-ion lignin-based lithium salt. [b] $Al(ClO_4)_3$+$Mg(ClO_4)_2$+PEO. [c] Zwitterionic cellulose nanofiber. [d] Silicone nanofilaments grafted montmorillonite nanosheets. [e] A crosslinked electrolyte consisting of fluoroethylene carbonate, methacrylate, triethylene glycol dimethacrylate,

and ethoxylated trimethylolpropane triacrylate. [f] Functionalized LLZTO+LiODFB+HPIB+PVDF. [g] A sustainable ion conductor by intercalating LiTFSI and SN into the interlayer space of montmorillonite nanosheets.

Table S2. Performances comparison of the CSEs based on SiO_2 in this work and recent studies.

Types	CSEs	Filler content	Ionic conductivity (mS cm^{-1}), T	t_{Li+}	Electrochemical stability window (V)	Cycling performance of Li/LFP cells	Refs.
Functionalized SiO_2	PEO/SE@$SiO_{2(200)}$	16.5%	0.62, 30 °C	0.81	4.3	97.0% capacity retention after 500 cycles at 1.0 C and 30 °C	This work
	PEO/PEGDA/LiTFSI-vinyl functionalized SiO_2	10%	0.0508, 60 °C	-	5.2	91% capacity retention after 300 cycles at 0.5 C and 60°C	[10]
	Superhydrophobic SiO_2	15%	0.43, 60 °C	0.5	5.0	93.8% capacity retention after 500 cycles at 1 C and 30 °C	[11]
Conventional SiO_2	PEO_{18}-LiTFSI-SiO_2-SN	5%	0.33, 60 °C	-	-	99% capacity retention after 100 cycles at 0.5 C	[12]
	PEO-LiTFSI-SiO_2	10%	0.435, 30 °C	0.65	5.0	83.4% capacity retention after 100 cycles at 0.1 C and 60 °C	[13]

	PEO/$LiClO_4$-SiO_2	15%	0.189, 25 °C	-	5.0	98.1% capacity retention after 50 cycles at 0.5 C and 60 °C	[14]
Mesoporous SiO_2	PEO/TMS-TFSISPE[a]@SiO_2	30%	1, 25 °C	0.9	-	-	[15]
	PEO-LiTFSI-PDA[b]@SiO_2	0.2%	0.189, 60 °C	0.293	5.33	97.2% capacity retention after 205 cycles at 0.2 C and 60°C	[16]
	PGME[c]-BMP-TFSI[d]@SiO_2	5%	1.4, RT	-	4.3	-	[17]
	PEG-LiTFSI-SiO_2	5.9%	0.0016, 30 °C	-	3.9	-	[18]
SiO_2 aerogels	SB[e]-PVDF/LiTFSI-SB-SiO_2	8%	0.055, RT	0.5	5.1	97.1% capacity retention after 200 cycles at 1 C	[19]
	PEG-UPy[f]/LiTFSI-SiO_2-UPy[g]	10%	0.0801, 30 °C	0.43	5.1	95.8% capacity retention after 60 cycles at 0.2 C and 60 °C	[20]
	PVA-SiO_2 aerogel	-	0.011, 18 °C	-	-	-	[21]
	PEO-SiO_2 aerogel	-	0.6, 30 °C	0.38	-	95% capacity retention after 200	[22]

						cycles at 0.5 C	
	$(PEO)_8$-$LiClO_4$-SiO_2	12%	0.022, 30 °C	-	-	-	[23]
In situ synthesized SiO_2	PEO-LITFSI-SiO_2	9.1%	0.18, 30 °C	0.42	5.3	88% capacity retention after 400 cycles at 0.5 C	[24]
	PEO-$LiClO_4$@SiO_2NP	10%	0.11, 30 °C	0.36	4.8	85.7% capacity after 100 cycles at 2 C and 90°C	[25]
	PEO-$LiClO_4$-nano-SiO_2	10%	0.044, 30 °C	-	5.5	91.7% capacity after 80 cycles at 1C and 90 °C	[26]

[a] 2-[(Trifluoromethanesulfonylimido)-*N*-4-sulfonylphenyl]ethyl trimethoxysilane. [b] Polydopamine. [c] Proprylene glycol monomethyl ether. [d] 1-Butyl-1-methylpyrrolidinium bis(trifluoromethylsulfonyl)imide. [e] Sulfonate betaine. [f] Ureido-pyrimidinone functionalized PEG. [g] Ureido-pyrimidinone functionalized SiO_2.

Table S3. Deconvolution parameters for $TFSI^-$ breathing region at 25 °C.

Samples	Peak center (cm^{-1})	Area (a.u.)	Assignment	R_{TFSI-}[a]	Fraction (%)
PEO/SiO_2	734.5	750.11	SSIP	14.15	6.60
	738.4	9172	CIP		80.71
	743.5	1442	AGG		12.69
PEO/SE@$SiO_{2(120)}$	734.1	1391	SSIP	5.72	14.89
	738.8	6052	CIP		64.78
	743.4	1900	AGG		20.34
PEO/SE@$SiO_{2(160)}$	734.0	1669	SSIP	4.81	17.20
	738.7	6700	CIP		69.06
	743.4	1333	AGG		13.74
PEO/SE@$SiO_{2(200)}$	734.6	2295	SSIP	2.79	26.41
	738.6	4685	CIP		53.92
	744.0	1709	AGG		19.67
PEO/SE@$SiO_{2(240)}$	734.5	3319	SSIP	3.26	23.47

	739.1	8938	CIP		63.21
	744.0	1884	AGG		13.32
	734.9	1283	SSIP		17.65
PEO/SE@$SiO_{2(280)}$	738.6	4230	CIP	4.67	58.18
	743.6	1757	AGG		24.17

[a] R_{TFSI-} means $TFSI^-$ coordination ratio, which can be calculated by the equation: $R_{TFSI-}=(A_{CIP}+A_{GG})/A_{free}$.

Table S4. Deconvolution parameters for C–O–C stretching band at 25 °C.

Samples	Peak center (cm^{-1})	Area (a.u.)	Assignment	R_{CO} [a]
PEO/SiO_2	1122.4	5567	Coordinated	0.23
	1140.7	24330	Non-coordinated	
PEO/SE@$SiO_{2(120)}$	1122.7	9163	Coordinated	0.44
	1140.9	20695	Non-coordinated	
PEO/SE@$SiO_{2(160)}$	1123.2	14693	Coordinated	0.55
	1140.7	26597	Non-coordinated	
PEO/SE@$SiO_{2(200)}$	1122.8	8249	Coordinated	0.68
	1141.2	12135	Non-coordinated	
PEO/se@$SiO_{2(240)}$	1122.5	10952	Coordinated	0.64
	1140.0	17073	Non-coordinated	
PEO/SE@$SiO_{2(280)}$	1122.4	17161	Coordinated	0.54
	1141.1	31515	Non-coordinated	

[a] Coordination ratio ($R_{CO} = A_{coord}/A_{non\text{-}coord}$).

Table S5. Deconvolution parameters for C-C-O and C-O-C stretching band at 25 °C.

Sample	Peak center (cm^{-1})	Area (a.u.)	Assignment	R_{cryst} [a]
PEO/SiO_2	842.0	8045	Random Coil Conformation	0.98
	858.7	8200	Helical Conformation	
PEO/SE@$SiO_{2(120)}$	841.8	8567	Random Coil Conformation	1.11
	859.2	7706	Helical Conformation	
PEO/SE@$SiO_{2(160)}$	842.1	21642	Random Coil Conformation	1.52
	859.1	14271	Helical Conformation	
PEO/SE@$SiO_{2(200)}$	842.0	13215	Random Coil Conformation	1.63
	858.9	8111	Helical Conformation	
PEO/SE@$SiO_{2(240)}$	842.2	14380	Random Coil Conformation	1.53
	859.2	9412	Helical Conformation	
PEO/SE@$SiO_{2(280)}$	842.0	11215	Random Coil Conformation	1.38
	858.9	8113	Helical Conformation	

[a] Raman crystallinity index.

Table S6. Cycling performance of Li/LFP cells with CSEs in this work and recent studies.

CSEs	Cycling performance of Li/LFP cells	Refs.
PEO/SE@$SiO_{2(200)}$	97.0% capacity retention after 500 cycles at 1 C and 30 °C 94.6% capacity retention after 80 cycles at 0.1 C and 0 °C	This work
PEO/GF/LiTFSI-SN	98.5% capacity retention after 100 cycles at 0.2C and 25°C	[27]
PEO/LiTFSI-LLZO	90.0% capacity retention after 200 cycles at 0.2C and 45°C	[28]
PEO/CM-LiTFSI-LLZTO	95.0% capacity retention after 500 cycles at 0.5C and 60°C	[29]
PEO/LiTFSI-LLZAO	81.0 % capacity retention after 200 cycles at 0.1 C and 60°C	[30]
PEO/LiTFSI-CeO_2	80.0 % capacity retention after 100 cycles at 0.2 C and 50°C	[31]
PEO/LiTFSI-LLZO	90.0 % capacity retention after 200 cycles at 0.5 C and 60°C	[32]
PAEV/LiFSI-ACMO	92.0% capacity retention after 300 cycles at 1 C and 50°C	[33]
PEO/PVDF-LiTFSI-LLZO	93.4 % capacity retention after 100 cycles at 0.2 C and 55°C	[34]
PEO/LiTFSI-OV-LLZTO	84.2% capacity retention after 1000 cycles at 5 C and 60°C	[35]

Movie S1. Powering a fan by the pouch cell, which highlights practical applicability of the PEO/SE@$SiO_{2(200)}$ CSE.

References

1. Y. Liu, P. Wang, Z. Yang, L. Wang, Z. Li, C. Liu, B. Liu, Z. Sun, H. Pei, Z. Lv, W. Hu, Y. Lu and G. Zhu, *Adv. Mater.*, 2024, 36, 2400970.
2. Y. Wei, T. H. Liu, W. Zhou, H. Cheng, X. Liu, J. Kong, Y. Shen, H. Xu and Y. Huang, *Adv. Energy Mater.*, 2023, 13, 2203547.
3. H. An, M. Li, Q. Liu, Y. Song, J. Liu, Z. Yu, X. Liu, B. Deng and J. Wang, *Nat. Commun.*, 2024, 15, 9150.
4. Y. Cheng, Z. Cai, J. Xu, Z. Sun, X. Wu, J. Han, Y. H. Wang and M. S. Wang, *Angew. Chem. Int. Ed.*, 2024, 63, e202400477.
5. W. Wang, Y. Yang, J. Yang and J. Zhang, *Angewandte Chemie International Edition*, 2024, 63, e202400091.
6. Q. Sun, S. Wang, Y. Ma, D. Song, H. Zhang, X. Shi, N. Zhang and L. Zhang, *Adv. Mater.*, 2023, 35, 2300998.
7. B. Yang, N. Chen, J. Tian, L. Sun, C. Deng, Y. Shang, Z. Liu, N. Wu, L. Zhao, F. Wu, D. Xia and R. Chen, *Adv. Mater.*, 2025, 37, 2415966.
8. W. Wang, Y. Yang and J. Zhang, *Nano Lett.*, 2025, 25, 3867−3874.
9. W. Yang, Y. Liu, X. Sun, Z. He, P. He and H. Zhou, *Angew. Chem. Int. Ed.*, 2024, 63, e202401428.
10. H. Zhan, M. Wu, R. Wang, S. Wu, H. Li, T. Tian and H. Tang, *Polymers)*, 2021, 13.
11. H. Luo, J. Yang, Y. Yang, W. Wang, W. Han and J. Zhang, *ACS Appl. Mater. Interfaces*, 2025, 17, 36763-36772.
12. W. Lyu, G. Q. He and T. Liu, *ChemistryOpen*, 2020, 9, 713-718.
13. J. Hu, W. Wang, X. Zhu, S. Liu, Y. Wang, Y. Xu, S. Zhou, X. He and Z. Xue, *J. Membr. Sci.*, 2021, 618, 118697.
14. X. Li, L. Yang, D. Shao, K. Luo, L. Liu, Z. Wu, Z. Luo and X. Wang, *J. Appl. Polym. Sci.*, 2019, 137.
15. Y. Kim, S. J. Kwon, H.-k. Jang, B. M. Jung, S. B. Lee and U. H. Choi, *Chem. Mater.*, 2017, 29, 4401-4410.

16. Y. Li, Y. Qin, J. Zhao, M. Ma, M. Zhang, P. Li, S. Lu, H. Bu, K. Xi, Y. Su and S. Ding, *ACS Appl. Mater. Interfaces*, 2022, 14, 18360-18372.
17. X. B. Chen, B. Put, A. Sagara, S. Mikinari, M. Maarten and M. V. Philippe, *Sci. Adv.,* 2020, 6, eaav3400.
18. K. Maouacine, C. Lebouin, E. T. Weldekidan, E. Ahiavi, R. Bouchet, D. Devaux, R. Denoyel and V. Hornebecq, *Microporous Mesoporous Mater.*, 2022, 345, 112236.
19. J. Lan, H. Hou, X. Yu, J. Rong and F. Chen, *Surfaces Interfaces*, 2023, 39, 102978.
20. B. Zhou, Y. H. Jo, R. Wang, D. He, X. Zhou, X. Xie and Z. Xue, *J. Mater. Chem. A*, 2019, 7, 10354-10362.
21. J. P. Vareda, A. C. Fonseca, A. C. F. Ribeiro and A. D. R. Pontinha, *Gels*, 2024, 10.
22. D. C. Lin, P. Y. Yuen, Y. Y. Liu, W. Liu, N. Liu, R. H. Dauskardt and Y. Cui, *Adv. Mater.*, 2018, 30, 1802661.
23. W. Wei, H. Zhang, X. Li, H. Zhang, Y. Li and I. Vankelecom, *Phys. Chem. Chem. Phys.*, 2013, 15, 1766-1771.
24. C. Wang, T. Q. Yang, W. K. Zhang, H. Huang, X. P. He and J. Zhang, *J. Mater. Chem. A*, 2022, 10, 3400-3408.
25. Z. Xu, T. Yang, X. Chu, H. Su, Z. Wang, N. Chen, B. Gu, H. Zhang, W. Deng, H. Zhang and W. Yang, *ACS Appl. Mater. Interfaces*, 2020, 12, 10341-10349.
26. D. Lin, W. Liu, Y. Liu, H. R. Lee, P. C. Hsu, K. Liu and Y. Cui, *Nano Lett.*, 2015, 16, 459-465.
27. J. Wang, J. Yang, L. Shen, Q. Guo, H. He and X. Yao, *ACS Appl. Energy Mater.*, 2021, 4, 4129-4137.
28. H. L. Nguyen, V. T. Luu, M. C. Nguyen, S. H. Kim, Q. H. Nguyen, N. I. Nungu, Y. S. Jun and W. Ahn, *Adv. Funct. Mater.*, 2022, 32, 2207874.
29. J. Song, Y. Xu, Y. Zhou, P. Wang, H. Feng, J. Yang, F. Zhuge and Q. Tan, *ACS Appl. Mater. Interfaces*, 2023, 15, 20897-20908.
30. J. Cheng, G. Hou, Q. Chen, D. Li, K. Li, Q. Yuan, J. Wang and L. Ci, *Chem. Eng. J.*, 2022, 429, 132343.
31. Q. Liu, T. Yu, H. Yang, S. Xu, H. Li, K. Chen, R. Xu, T. Zhou, Z. Sun and F. Li, *Nano Energy*, 2022, 103.
32. S. Guo, W. Kou, W. Wu, R. Lv, Z. Yang and J. Wang, *Chem. Eng. J.*, 2022, 427, 131948.
33. Z. Tian, L. Hou, D. Feng, Y. Jiao and P. Wu, *ACS Nano*, 2023, 17, 3786-3796.

34. H. Zhuang, W. Ma, J. Xie, X. Liu, B. Li, Y. Jiang, S. Huang, Z. Chen and B. Zhao, *J. Alloys Compoun.*, 2021, 860, 157915.

35. Y. Fu, K. Yang, S. Xue, W. Li, S. Chen, Y. Song, Z. Song, W. Zhao, Y. Zhao, F. Pan, L. Yang and X. Sun, *Adv. Funct. Mater.*, 2023, 33, 202210845.